Computers and Electronics in Agriculture 66 (2009) 147–158

Contents lists available at ScienceDirect

Computers and Electronics in Agriculture

journal homepage: www.elsevier.com/locate/compag

Sieveless particle size distribution analysis of particulate materials through computer vision

C. Igathinathane[a,*], L.O. Pordesimo[a], E.P. Columbus[a], W.D. Batchelor[a], S. Sokhansanj[b]

[a] Agricultural and Biological Engineering Department, 130 Creelman Street, Mississippi State University, Mississippi State, MS 39762, USA
[b] Oak Ridge National Laboratory, Environmental Sciences Division, Oak Ridge, P.O. Box 2008, TN 37831, USA

ARTICLE INFO

Article history:
Received 25 July 2008
Received in revised form
28 December 2008
Accepted 14 January 2009

Keywords:
Biomass sieve analysis
Dimension
ImageJ plugin
Image processing
Particle size distribution
Physical property

ABSTRACT

This paper explores the inconsistency of "length-based separation" by mechanical sieving of particulate materials with standard sieves, which is the standard method of particle size distribution (PSD) analysis. We observed inconsistencies of length-based separation of particles using standard sieves with manual measurements, which showed deviations of 17–22 times. In addition, we have demonstrated the "falling through" effect of particles cannot be avoided irrespective of the wall thickness of the sieve. We proposed and utilized a computer vision with image processing as an alternative approach; wherein a user-coded Java ImageJ plugin was developed to evaluate PSD based on length of particles. A regular flatbed scanner acquired digital images of particulate material. The plugin determines particles lengths from Feret's diameter and width from pixel-march method, or minor axis, or the minimum dimension of bounding rectangle utilizing the digital images after assessing the particles area and shape (convex or nonconvex). The plugin also included the determination of several significant dimensions and PSD parameters. Test samples utilized were ground biomass obtained from the first thinning and mature stand of southern pine forest residues, oak hard wood, switchgrass, elephant grass, giant miscanthus, wheat straw, as well as Basmati rice. A sieveless PSD analysis method utilized the true separation of all particles into groups based on their distinct length (419–639 particles based on samples studied), with each group truly represented by their exact length. This approach ensured length-based separation without the inconsistencies observed with mechanical sieving. Image based sieve simulation (developed separately) indicated a significant effect ($P < 0.05$) on number of sieves used in PSD analysis, especially with non-uniform material such as ground biomass, and more than 50 equally spaced sieves were required to match the sieveless all distinct particles PSD analysis. Results substantiate that mechanical sieving, owing to handling limitations and inconsistent length-based separation of particles, is inadequate in determining the PSD of non-uniform particulate samples. The developed computer vision sieveless PSD analysis approach has the potential to replace the standard mechanical sieving. The plugin can be readily extended to model (e.g., Rosin–Rammler) the PSD of materials, and mass-based analysis, while providing several advantages such as accuracy, speed, low cost, automated analysis, and reproducible results.

Published by Elsevier B.V.

1. Introduction

Accurate and rapid particle size distribution (PSD) analysis is desirable in various fields that handle granular or particulate materials. The PSD measurement is generally carried out by mechanical sieving utilizing a standard sieve set, which is considered as a standard procedure. The other existing methods of PSD measurement utilize the principles of light scattering, acoustic spectroscopy, and laser diffraction. These advanced instruments are highly expensive and often assume a spherical geometry for the irregular sample particles in the analysis. The American Society of Agricultural and Biological Engineers (ASABE Standards S424.1, 2007) adopted PSD analysis to determine and express the particle size of chopped forage materials by mechanical screening. In general, results from PSD analysis include percentage of particles retained on different sized sieves, cumulative undersize distribution, arithmetic and geometric mean dimension and associated standard deviation, and several other parameters that uniquely describe the PSD. Comparison of the PSD parameters of input feed and output product quantifies effectiveness of the size reduction process itself as a function of new surfaces generated. Furthermore, the PSD results can be correlated to the energy expended in size reduction thereby serving as a performance indicator to evaluate different size reduction equipment.

Mechanical sieving with standard sieves has several issues such as the process involves expensive mechanical shaker and standard sieves, requires guesswork in selection of sieve set, consumes time,

* Corresponding author. Tel.: +1 662 325 3365; fax: +1 662 325 3853.
E-mail addresses: igathi@gmail.com, igathi@abe.msstate.edu (C. Igathinathane).

0168-1699/$ – see front matter. Published by Elsevier B.V.
doi:10.1016/j.compag.2009.01.005

and limits the sieve selection to only a finite set (56 sieves complete) of available standard sieves (Igathinathane et al., 2008a). Blott and Pye (2001) reported that the calculations of PSD statistics for many samples can be a laborious process; and developed a computer program called GRADISTAT for the rapid analysis of grain size statistics from any of the standard measuring techniques, such as sieving and laser granulometry. They described the fundamentals of grain size analysis, and presented various statistical formulae used in the calculation of grain size parameters and suggested descriptive terminology. Mechanical sieving may also result in unbalanced separation of particles on sieves. The limitations of sieving equipment constrain the PSD analysis of a particulate sample, which is a collection of hundreds of distinct dimensioned particles, with the available data from 7 to 15 sieves thereby restricting dimensional measurement accuracy.

A computer vision based image processing method can be considered as an alternative or even a replacement for sieve analysis. Brosnan and Sun (2002) reviewed the various machine vision research areas that include inspection, grading, classification, and analysis of several agricultural and food products. They also reported the merits and drawbacks of machine vision systems and suggested future research approaches in the field. Reported studies on determining size as well as size distribution using digital image processing of variety of materials include circular particles (Momota et al., 1994), rock crusher aggregates (Maerz, 1998), coarse aggregates (Mora et al., 1998), rain drops (Cruvinel et al., 1999), and food grains and biomass particles (Igathinathane et al., 2008b, 2009).

The two basic requirements of computer vision digital image based size and size distribution analysis are an input image and an image processing algorithm. Devices for image acquisition include digital cameras, charge-coupled device cameras (Visen et al., 2004) or flatbed scanners (Shahin et al., 2006; Igathinathane et al., 2008a,b, 2009). For better results with image preprocessing, clear contrast between particles and background is essential. Arrangement of the particles with respect to one another other is another vital aspect. A singulated arrangement of particles (disjoint particles without overlap or touching one another) makes the preprocessing algorithm simpler avoiding the need for specialized singularization algorithms like watershed or successive erosion and dilation (Shahin and Symons, 2005).

Most of the machine vision applications reported in the literature use proprietary software because of their built-in image analysis capabilities. This convenience, of course, comes at a price. A surprising option is ImageJ. ImageJ is a free image processing and analysis program that can be utilized to develop user-coded plugins to suit the specific requirements of any conceived application. ImageJ is a Java-based public domain image processing and analysis program developed at the National Institutes of Health (NIH), USA, which is freely available, open source, multithreaded and platform independent with tools for user-coded macro and plugin development (Bailer, 2006; Rasband, 2007; Burger and Burge, 2008). Igathinathane et al. (2008b) developed an ImageJ plugin to determine the dimensions of singulated particles by identifying their shapes and analyze their size distribution. Their other ImageJ applications plugin include (1) a more robust method of "pixel-march" to determine the orthogonal dimensions of convex shaped food grains (Igathinathane et al., 2009) and (2) simulation of mechanical sieve analysis of ground biomass materials (Igathinathane et al., 2008a).

This present research aims to address issues associated with mechanical sieving through computer vision approach. This research proposes to develop a sieveless PSD analysis method through a user-coded ImageJ plugin that directly determines the PSD (without sieves) based on the dimensions of distinct particles in samples of particulate material. Specific objectives of this research were to:

1. Demonstrate the inconsistency of length-based separation by standard sieves—to emphasize the necessity and value of a computer vision approach.
2. Develop a user-coded ImageJ plugin based on determined distinct lengths of all particles to analyze PSD and determine various PSD parameters.
3. Apply the sieveless analysis plugin to evaluate PSD and its parameters for samples of ground biomass and rice grains.
4. Determine the effect of number of virtual sieves by simulation with respect to sieveless analysis involving all distinct particles.

2. Materials and methods

2.1. Test materials

Ground biomass served as the primary test materials, and we selected pine species (*Pinus* spp.) of first thinning (14-year old) and mature stand (54-years old) southern pine forest residues (SPFR), oak hard wood (*Quercus* spp.), switchgrass (*Panicum virgatum*), elephant grass (*Pennisetum purpureum*), giant miscanthus (*Miscanthus floridulus*), and wheat straw (*Triticum aestivum*). These materials in dry condition were hammer milled through a 6.35 mm (1/4″) diameter screen. A Boerner-type seed divider (Seedburo Equipment Co., Chicago, IL, USA) divided these input material into representative samples that were used in image acquisition. Analysis was extended to a more uniform sample such as whole Basmati rice grains to contrast and demonstrate the versatility and range of the plugin.

2.2. Procedure of image acquisition and preprocessing

A flatbed scanner (4800 × 9600 DPI; Cano-scan 4400F, Canon USA. Inc., Lake Success, NY, USA) acquired the color image of the test materials. Particles were well spread in singulated arrangement where a thin layer of material is laid in a manner that particles do not touch or overlap one another. However, when particles are very minute it will be difficult to avoid occasional deviation from singulated arrangement. Resolving particles touching one another involved advanced techniques, for example, successive erosion-scrap-dilation sequence (Shahin and Symons, 2005). For simplicity sake, we considered only singulated arrangements of particles, which forces particles touching each to be considered as a single particle. Although singulated arrangements required additional effort in spreading the particles, it simplified the image preprocessing and improved the dimensional measurement. The scanning software allows to custom scan images with user-defined dots per inch (DPI) value. All the images were scanned at 300 DPI on both horizontal and vertical direction.

Image preprocessing essentially involves the creation of binary image of the particles from color images before being processed by the application algorithm. ImageJ tools convert original color image first to grey-scale (8-bit) image, then to binary image based on user input threshold limits. Inbuilt commands of ImageJ such as "*8-bit*" and "*Threshold. . .*" performed these preprocessing tasks. For threshold limit setting, the lower and upper limits were adjusted so that the particles of interest are judiciously covered. The "*Auto-threshold*" served as a good guide. We used in this work a constant threshold range from 70 to 255 for all the images. When the plugin was run, it invokes the ImageJ "*Analyze Particles*" routine, which generates the basic dimensions of the particles. In the final "*Analyze Particles*" dialog, particle areas to be considered were set as 0 to infinity (covering all particles) pixel units, and the options such as "*Exclude on Edges*" and "*Include Holes*" were selected to ensure coverage of the whole particles, and the exclusion of holes, if any, in the particles of the image.

2.3. Image calibration

Proper calibration procedure in an image processing application is crucial to ensure plugin portability and account for variations in image input devices and user platforms. The calibration procedure essentially determines a scale factor, which converts the pixel units of the image to physical units of dimensions (e.g. mm). The scale factor was obtained from the image DPI information—a measure of image resolution. Image file "*Properties*" or the scanning software provides the DPI value. The scanned image resolution of 300 DPI corresponds to a constant scale factor of 0.0847 mm/pixel.

The plugin was coded in such a way that the calibration is required only once at the start of a multiple plugin execution or as and when required. The calculated scale factor in the initial session was stored in a text file and subsequent measurements retrieved it from the stored file, without having to input the DPI value again. The scale factor used in this study may change with other image resolutions.

2.4. Particle size distribution plugin development

2.4.1. Background on particle size determination from digital images

Including ImageJ, various particle analysis software map the actual particle projected profile to an equivalent ellipse (Rodieck, 2008) so that both area and perimeter match. Some of the ImageJ built-in commands for particle analysis outputs are number of particles, area, perimeter, width and height of bounding rectangle, major and minor axes of best-fitting ellipse, angle of inclination of the major axis with the horizontal, and Feret's diameter.

The maximum dimension of the particle, termed as "length" hereafter, is the dominant and most significant dimension of the particle. Therefore length-based classification of particles produces proper grouping and subsequently analyzed for PSD. A physical classification method such as mechanical sieving as well seeks to classify the particles based on the sieve opening dimensions. Hence, it is essential to develop strategies to determine the length as well as width of particles and analyze PSD from the digital images.

2.4.2. Particle length determination

A closer examination of ground biomass material reveals that they are of irregular shape with pointed edges due to the shredding action of the size reduction machinery. Although shapes of finer particles tend to be convex polygonal, the larger particles tend to deviate and be nonconvex polygonal. A simple yet traceable and reproducible method of particle length determination is utilizing the Feret's diameter, included in ImageJ as standard output. The Feret's diameter is the diameter of a smallest circle that encloses a particle outline, which actually signifies the particle's maximum dimension (Fig. 1).

The application of Feret's diameter produces length overestimation only with some geometrically shaped particles such as rectangles and squares, where the maximum dimension belongs to the diagonal. However, length based on Feret's diameter has relevance in sieving based classifications. Diagonal dimensions of square sieve often designate sieve openings as well as used in PSD analysis. The Feret's diameter was also directly related to the material flow through circular sieves, where the maximum particle dimension determines whether a particle is retained or fall through a sieve. For natural particles, such as ground biomass of both convex and nonconvex shapes with rough edges, the Feret's diameter can correctly represent the particle length.

2.4.3. Particle width determination—pixel-march method

Igathinathane et al. (2008a, 2009) reported a pixel-march method for measuring dimensions of convex shaped particles from

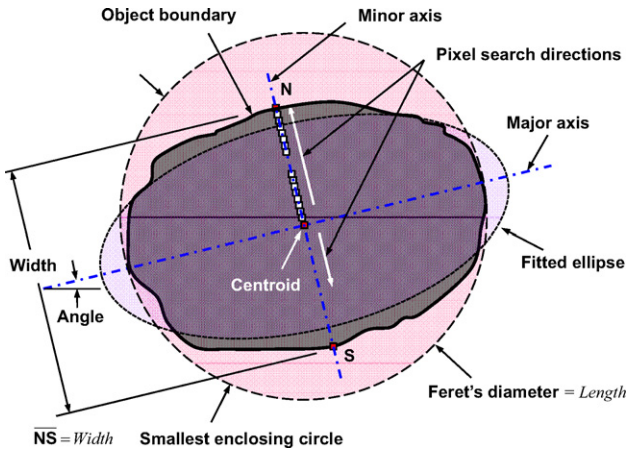

Fig. 1. Feret's circle method of length and pixel-march method of width determination.

binary digital images. The pixel-march method essentially measures the width of the particles by locating the boundary while marching outward from the centroid of the object by searching the pixel color (Fig. 1). ImageJ fitted ellipse parameter, namely the minor axis, guides the search process. To locate the boundary pixels, the color of current pixel was assessed by "pointCol = ip.get(x,y);" statement, while marching along the minor axis utilizing the calculated slope. In the thresholded binary image, a pixel color value of 255 (black) signals the marching point lies within the particle boundary, and a value of 0 (white) outside the boundary. Thus marching from the particle's centroid determines the coordinates of particle boundary points along minor axis (N and S) (Fig. 1). From these boundary points coordinates (N and S), the width of the particle was determined using the distance formula. The pixel-march for orthogonal dimensions is 96.6% accurate (Igathinathane et al., 2008a,b), and it works well with convex irregular shapes. This method can be likened to the action of inside calipers in measuring object's inner dimensions.

When the particles were minute, with their areas represented by fewer than nine pixels, clear representation of major and minor axes cannot be obtained. Therefore, for such particles the bounding rectangle dimensions from ImageJ standard outputs were considered to represent the width. The minimum of width or height of the bounding rectangle was assigned as the width of particle, and this arrangement accommodated various orientations of the particles.

The pixel-march method will not work with nonconvex (curved or twisted shapes, e.g. fibrous biomass) particles, where the centroid falls outside the object boundary. Therefore for nonconvex particles, identified by the white color of the centroid coordinates, the minor axis was assigned to width for simplicity sake. It is understood that the minor axis cannot be as accurate as the pixel-march based width. Dealing with the nonconvex particles may require further programming to handle all possible situations. However, as shown in results, the percentages of nonconvex shaped particles with ground material were limited. Finally for nonconvex particles, the minimum of the different options for width (bounding rectangle dimensions and minor axis) was assigned.

2.5. Sieveless particle PSD analysis

Unlike mechanical sieving, where particles are classified based on a limited number of sieves, this research employs classification based on numerous distinct length particles from the image without sieves. The determined lengths of all the particles can be categorized into several particles of distinct lengths. With the limitations of the input device resolution, many particles lengths will

match and were uniquely grouped based on their distinct lengths. The grouping of particles represented by each distinct length particle actually makes up the total number of particles of the sample. This method of grouping particles of distinct lengths, obtained without sieves by computer vision, is essentially equivalent to the action of sieves separating and grouping the particles mechanically. The number of grouped particles can be subsequently subjected to cumulative undersize characteristics, and evaluation of various PSD parameters to complete the PDS analysis.

2.6. PSD analysis and parameters

Dimensions of significance based on length, such as D_{95}, D_{90}, D_{84}, D_{75}, D_{60}, D_{50}, D_{30}, D_{25}, D_{16}, D_{10}, and D_5 describing the particle size and their distribution were derived from the cumulative undersize characteristics of particle dimensions original data. The following several common PSD parameters based on length were evaluated from these significant dimensions. Uniformity index, size guide number, and size range variation coefficient (CFI, 2001; EBA, 1997; Allaire and Parent, 2003), relative span (Allais et al., 2006), coefficient of uniformity and coefficient of gradation (Craig, 2004); and graphic mean, inclusive graphic standard deviation, inclusive graphic skewness, and graphic kurtosis (Folk and Ward, 1957; Blott and Pye, 2001) were evaluated as:

$$I_u = \frac{D_5}{D_{90}} \times 100 \tag{1}$$

$$N_{sg} = D_{50} \times 100 \tag{2}$$

$$S_v = \frac{D_{84} - D_{16}}{2D_{50}} \times 100 \tag{3}$$

$$S_l = \frac{D_{90} - D_{10}}{D_{50}} \tag{4}$$

$$C_u = \frac{D_{60}}{D_{10}} \tag{5}$$

$$C_g = \frac{D_{30}^2}{D_{10} \times D_{60}} \tag{6}$$

$$X_g = \frac{D_{16} + D_{50} + D_{84}}{3} \tag{7}$$

$$\sigma_{ig} = \left[\frac{D_{84} - D_{16}}{4}\right] + \left[\frac{D_{95} - D_5}{6.6}\right] \tag{8}$$

$$S_{ig} = \left[\frac{D_{84} + D_{16} - 2D_{50}}{2(D_{84} - D_{16})}\right] + \left[\frac{D_{95} + D_5 - 2D_{50}}{2(D_{95} - D_5)}\right] \tag{9}$$

$$K_g = \left[\frac{D_{95} - D_5}{2.44(D_{75} - D_{25})}\right] \tag{10}$$

where I_u is the uniformity index, dimensionless (%); N_{sg} is the size guide number, mm; S_v is the size range variation coefficient, dimensionless (%); S_l is the relative span based on length, dimensionless; C_u is the coefficient of uniformity, dimensionless; C_g is the coefficient of gradation, dimensionless; X_g is the graphic mean, mm; σ_{ig} is the inclusive graphic standard deviation, mm; S_{ig} is the inclusive graphic skewness, dimensionless; K_g is the graphic kurtosis, dimensionless; and D_{95}, D_{90}, D_{84}, D_{75}, D_{60}, D_{50}, D_{30}, D_{25}, D_{16}, D_{10}, and D_5 are the corresponding particle lengths in mm at respective 95%, 90%, 84%, 75%, 60%, 50%, 30%, 25%, 16%, 10%, and 5% cumulative undersize, which are also known as percentiles. The parameter C_g is also known as coefficient of curvature or coefficient of concavity, the D_{10} value as effective size (Craig, 2004), and D_{50} as median diameter. The graphic measures X_g, σ_{ig}, and S_{ig} were after Folk and Ward (1957) and were in most common use in sediment analysis (Blott and Pye, 2001).

We have also used ASABE Standards S424.1 (2007) method of determining and expressing particle size of chopped forage materials by screening to represent the whole distribution in terms of geometric mean length and associated standard deviation. This standard assumes that the mass distribution of all chopped forage materials is logarithmic normally distributed. Notwithstanding the log-normal distribution assumption, which several particulate materials deviate, this analysis is often used by researchers. In the present sieveless all distinct particles analysis, the number of particles replaced the mass of material, and distinct lengths of the particles replaced the nominal sieve aperture size of the *i*th sieve. Therefore the particles size were reported in terms of geometric mean length and associated standard deviation based on particle length are:

$$X_{gl} = \ln^{-1}\left[\frac{\sum(N_i \times \ln X_i)}{\sum N_i}\right] \tag{11}$$

$$\sigma_{gl} = \ln^{-1}\left[\frac{\sum(N_i(\ln X_i - \ln X_{gl})^2)}{\sum N_i}\right]^{\frac{1}{2}} \tag{12}$$

where X_{gl} is the geometric mean length of particles based on length, mm; N_i is the number of particles of a particular distinct dimension, dimensionless; X_i is the distinct length of particle, mm; and σ_{gl} is the standard deviation of geometric mean length of particles based on length, mm.

2.7. Calculation procedure and plugin coding

The particles were identified from left to right and top to bottom of the binary image, and their dimensions were determined and stored in arrays. The "bubble sort" algorithm sorted the stored length array. The number of particles of distinct lengths was always observed to be less than the total number of particles. This is because several particles will have coinciding lengths as the incremental length was based on single pixel dimension. Percent of distinct length particles was evaluated from the total number of particles. Cumulative undersize of each distinct length particles was calculated, after adding the number of all particles that were smaller than a particular distinct length and subtracting from 100.

The significant dimensions (D_5 through D_{95}) were evaluated from the corresponding length ranges of cumulative undersize data by linear interpolation. These dimensions were in turn used to calculate the PSD parameters (Eqs. (1)–(10)). The geometric mean length (X_{gl}) and associated standard deviation (S_{gl}) were evaluated separately in a "FOR" loop utilizing ASABE Standards S424.1 (2007) method (Eqs. (11) and (12)), after sorting the particle lengths.

The plugin coding followed the overall process flow as depicted in the form of a flowchart (Fig. 2). Java source code of the plugin was divided into several logical methods (procedure modules) of unique objectives, following the various indicated processes. The main "void run (ImageProcessor ip)" method simply calls these methods in proper sequence to execute the plugin. Even though the plugin is composed of only 1287 lines of source code, several Java and ImageJ classes imported and inherited would actually represent several hundred lines of codes used in the plugin—a definite advantage of object oriented programming approach.

2.8. Effect of number of sieves by simulation and statistical analysis

It would be worthwhile to know how many sieves will be required to statistically match the PSD results of sieveless analysis based on distinct particles. Since mechanical sieve shakers have limitation on the number of sieves that can be accommodated in the nest, the sieve simulation approach with virtual sieves was fol-

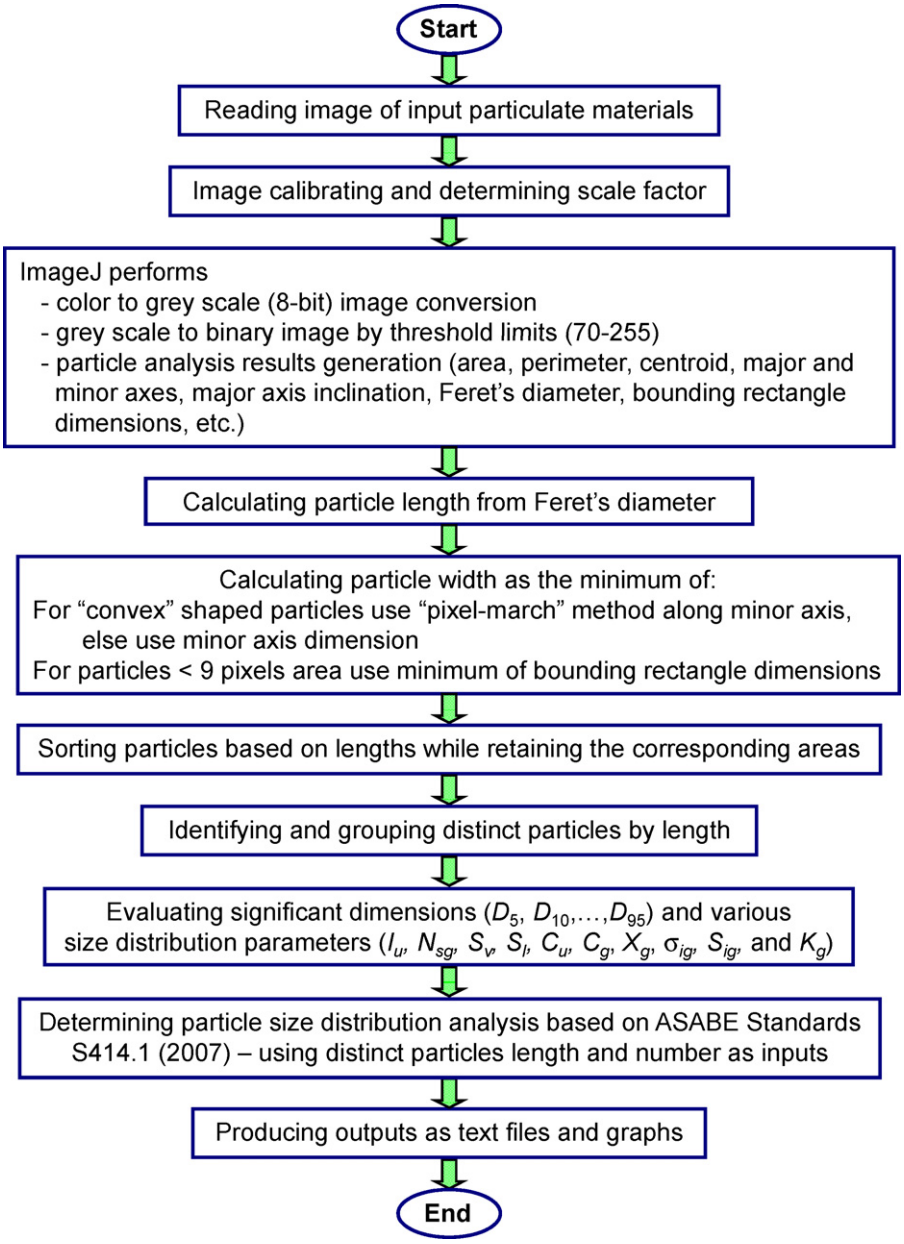

Fig. 2. Flowchart of sieveless all distinct particles particle size distribution analysis ImageJ plugin.

lowed. Sieve simulation with a fixed number of virtual sieves of known equally spaced opening dimensions involves grouping of particles based on their lengths corresponding to the selected sieve openings. For instance: a sieve simulation with three sieves will divide the particles into four groups, the first three groups represent particles retained on the three sieves and the fourth group represents particles passed through the 3rd sieve and that collected in pan. The dimensions of the equally spaced simulated sieves were obtained by dividing the total particle length range by 4 and allotting sieve dimensions progressively. In essence, the sieve simulation is simply mathematically grouping numbers indicating particle lengths based on number ranges indicating selected virtual sieve dimensions.

The number of virtual sieves considered in the simulation was 3, 4, 5, 7, 10, 15, 20, 30, 50, 75 and 100. Results of a similar sieve simulation along with experimental verification with mechanical sieving can be found in Igathinathane et al. (2008a). In contrast, the present sieveless PSD analysis performs complete separation and grouping of all particles based on distinct lengths, which can be thought of employing an equivalent number of virtual sieves ($\geq$419, as discussed later).

Effect of number of simulated sieves in comparison with sieveless all distinct particles PSD was evaluated statistically by mean separation analysis. A mixed model analysis of variance SAS macro "%manova" (Saxton, 2003) with log transformation and Tukey–Kramer ($P < 0.05$) mean separation analysis was utilized. Since the analysis requires data replications, we used a random $\pm$5% variation to generate two additional replication data on PSD parameters (Eqs. (1)–(11)). We resorted to this data generation as we used only one image per material. Alternatively, multiple images of the sample would have produced the data for mean separation analysis. Graphically, the effect of number of simulated sieves with reference to sieveless approach in representing PSD can be easily observed from the cumulative undersize distribution plots.

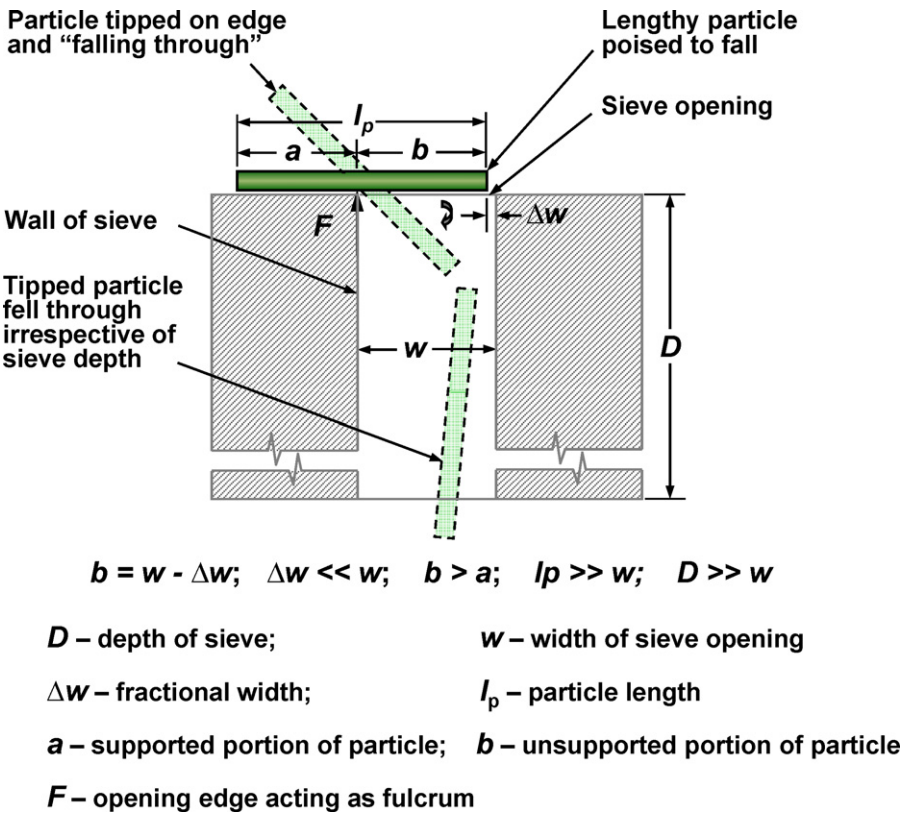

Fig. 3. Illustration of "falling through" effect of long particles through sieve openings by the action of gravity.

3. Characteristics of mechanical sieving

3.1. Length-based separation inconsistencies in mechanical sieving

The square or circular openings of standard sieves, in the strictest sense, will only allow "width-based separation" of particles. That is, these openings truly restrict particles of width larger than the sieve opening dimension irrespective of particle orientation with respect to the openings (Igathinathane et al., 2008a). However, utilizing standard sieves for particle length-based separation will lead to separation inconsistencies; because, square or circular openings will not prevent "falling through" or "nose diving" effect of lengthier particles passing through smaller sized sieve openings. Measures like increasing the sieve thickness, by punching holes from thick sheets of metal, were adopted by ASABE Standards S424.1 (2007) to overcome the "falling through" effect. It is expected that these deeper walls of sieve opening help restrict the easier passing of lengthier particles, but our observations show otherwise.

It can be easily visualized that this thick wall sieve design cannot truly resist the passage of lengthier particles when they tip at the edge of opening and subsequently fall through. A lengthy particle that is slightly smaller than twice the size of sieve opening, will fall through the sieve under the action of gravity, when the unsupported length is greater than the supported length (Fig. 3). The edge of the sieve opening will act as the fulcrum; and the walls of the sieve opening, irrespective of its thickness, cannot stop the tipping of particles even in static conditions. Variation in density along the length of the particle, due to uneven thickness, also influences the passage of particles. Independent of supported length, the particle will fall through when the unsupported portion is heavier. Dynamics of particle passage varies when the sieves are in motion, and the movement may enhance or reduce the chance of the "falling through" effect.

It can be also envisioned that any particles of width (or diameter in the case of rod-shaped particles) greater than sieve opening (w) cannot pass through the sieve in any orientation, which illustrates the true "width-based separation." In addition, with some ground material such as food grains, whose particles approaches spherical shape, the sieves will correctly separate these particles, as length and width coincide for spherical particles. However, the outlined mechanism (Fig. 3) illustrates the possibility of inconsistencies in length-based separation by sieves regardless of the sieve thickness.

Womac et al. (2007) observed this length-based separation inconsistency in particles size analysis of knife-milled ground corn stover, switchgrass, and wheat straw using ASABE design sieves (ASABE Standards S424.1, 2007) with thicker walls. Their measurements of particle length with a digital caliper were roughly five times greater than the geometric mean dimensions calculated from sieving results. Based on their results, they emphasized that sieve analyses of irregular shaped particles offer only relative comparisons, and that actual dimensions of particles retained on sieves are not necessarily represented by sieve opening sizes above and below the sample.

3.2. Demonstration of mechanical sieving length-based separation inconsistencies

To verify the length-based separation inconsistency, an analytical vibratory sieve shaker (Model AS200 digit, Retsch GmbH, Haan, Germany) was utilized for sieving ground first thinning SPFR. Hand-picked sub-samples retained over different sieves are shown in Fig. 4. The average length of these selected particles passing through the 1.4 mm (ASTM# 14) sieve was 23.3 ± 5.1 mm, and that passing through 0.71 mm (ASTM# 25) sieve was 15.8 ± 3.1 mm. These length measures were approximately 17 and 22 times the 1.4 and 0.71 mm actual opening dimensions of the standard sieves, respec-

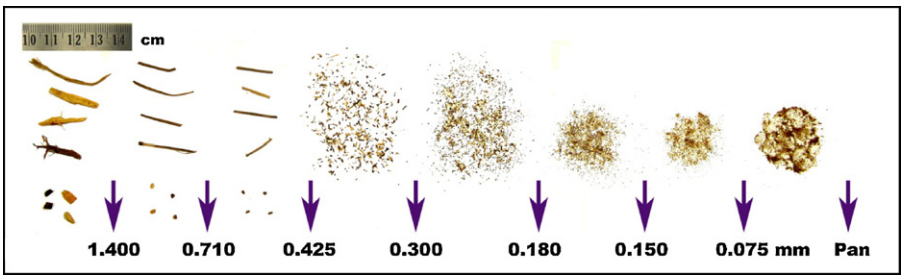

Fig. 4. Inconsistencies of particle length-based separation by sieves of square openings demonstrating "falling through" effect.

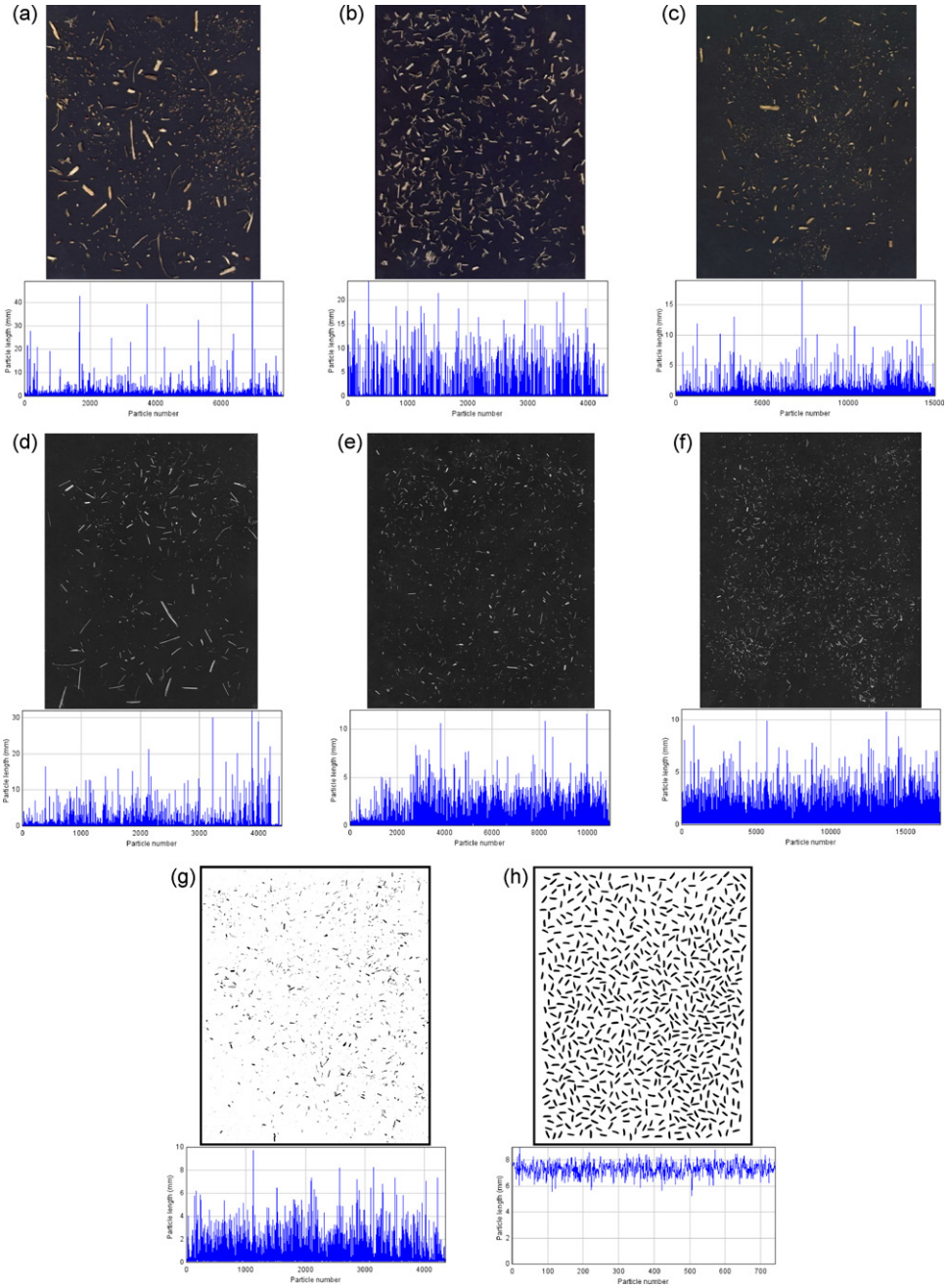

Fig. 5. Sample images of ground biomass and rice grains that were scanned from left to right and top to bottom to determine individual particle lengths: (a) first thinning SPFR, (b) mature stand SPFR, (c) oak hard wood, (d) miscanthus, (e) switchgrass, (f) elephant grass, (g) wheat straw, and (h) Basmati rice; a, b, and c represent original color images; b, c, and d represent preprocessed grey-scale images; and g and h represent processed binary images.

tively. However, most of the retained particles lengths were actually between the long and small particles as illustrated in the first three cases in Fig. 4. It should be noted that these particles, although hand-picked, demonstrate the possibility of inconsistent separation based on length by mechanical sieving. Similar disparity can be also observed with particles retained on other sieves of the set. Such inconsistencies were as well observed with other samples, thereby emphasizing the length-based separation inconsistency as a definite feature of mechanical sieving.

4. Results

4.1. Sample particle lengths through computer vision

The sample images were processed through the developed plugin and the particle lengths are presented in Fig. 5. Since the scanning and the measurement proceeds from left to right and top to bottom of the image, the plotted lengths can be traced back to specific particles in the image using the labeling feature of ImageJ. The processed images had the unique advantage of directly observing the overall spread of length enabling a better guess on the average particle length. This educated guess with the accuracy possible from computer processed images is not always possible by manual estimation. Furthermore, the complete measurement of length and width of all particles comprising the sample as performed by the plugin is virtually impossible through manual measurements.

It can be readily seen from the first thinning and mature stand SPFR (Fig. 5a and b) that several particle lengths were greater than 5 mm. In the other biomass samples (Fig. 5c–g) the particle lengths were predominantly less than 5 mm. All the biomass samples had very fine particles ($\leq$2 mm), as the particle length plot starts immediately after the *x*-axis. It is quite obvious that the particle lengths of Basmati rice (Fig. 5h) were uniform and mostly in the range of 6–8 mm. Absence of fines with Basmati rice is evident from the particle length plot staying well above *x*-axis, unlike the ground biomass samples.

4.2. Results of samples PSD from sieveless analysis

Particulate material PSD characteristics are in general expressed as plots of particle dimensions versus particle numbers and as a cumulative undersize distribution versus particle dimensions. These PSD characteristics provide overall information about the particles dimensions distribution graphically at a glance, and also enable to derive several distribution related numerical parameters describing the sample (Section 2.6). The PSD of materials studied showing all particles with their lengths sorted in descending order versus particle number of the sieveless analysis (Fig. 6). For all the biomass materials studied, the maximum particle

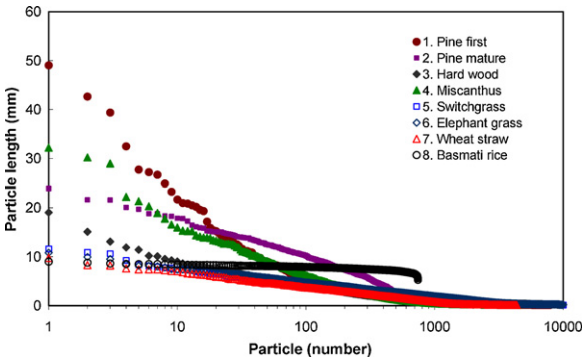

Fig. 6. Semi-log plot of sorted lengths of all particles of different samples.

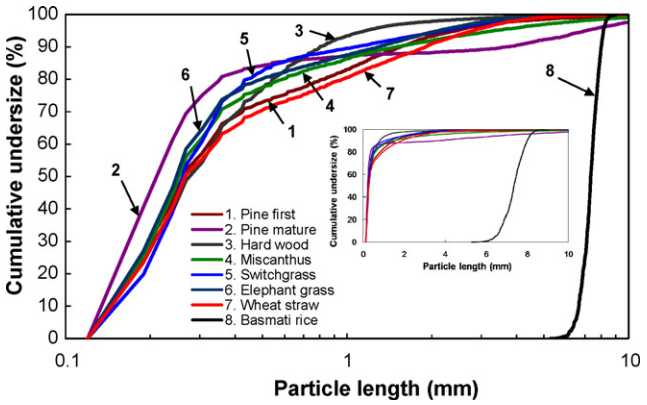

Fig. 7. Cumulative size distribution of sorted lengths of particles (semi-log plot) of different samples (Insert: Linear plot of cumulative size distribution).

length varied from 9.7 to 49.0 mm, and the minimum particle length of 0.12 mm. However, the maximum particle length range after the initial 50 particles was reduced as 4.5–12.5 mm, after 100 particles it was 3.7–10.2 mm, and after 200 particles it was 2.8–7.4 mm. These observations indicated the increased presence of finer particles. The Basmati rice grains were more uniform as indicated by a consistent and narrow particle length band (Fig. 5h). The length variation in the total range of 5.3–9.0 mm only, demonstrates the length uniformity. The semi-log plot (Fig. 6) spreads the data in the lower particle number range or particles of longer lengths, for easy observation. When plotted in linear scale (not shown), the quick reduction in particle lengths and asymptotic trend of length after 1000 particles can be readily observed.

Cumulative undersize versus particle length PSD curve was plotted for two log cycles to show in detail the variation of distinct particles of the sample (Fig. 7). This two log cycles (0.1–10 mm) account for most of the variation (97.6%) of all the materials studied, because the number of distinct particles longer than 10 mm for all the biomass samples was only 197 (4.8%) out of total 4094. It should be stated again that in the cumulative undersize curve, some of the data points may represent a group of particles of the same distinct length. For example, pine mature had 1759 (40.68%) particles of length 0.120 mm corresponding to 0.00% cumulative undersize, followed by 887 (20.51%) particles of 0.189 mm with 40.68% cumulative undersize, and 358 (8.28%) particles of 0.239 mm with corresponding cumulative undersize of 61.19%.

The cumulative undersize distribution when plotted on linear scale showed the quick increase and the curve stayed asymptotic to the 100% level (Fig. 7 insert). Ground biomass particles displayed most of the significant increase in cumulative undersize within particle length of 2 mm. Nature of cumulative undersize curve of Basmati rice (sigmoid shape) is totally different from the ground biomass particles as seen from both log and linear scales. The sigmoid shape in cumulative undersize plot signified a normal distribution of lengths for Basmati rice. The Basmati rice samples showed only a little variation since the particles were uniform and had a mean length of 6.919 ± 0.531 mm.

4.3. PSD parameters from sieveless analysis

Several significant dimensions from the PSD and the calculated parameters (Eqs. (1)–(10)) along with plugin performance are presented in Table 1. Images of ground biomass samples, while resulting from just a few grams of material, were comprised of thousands of particles (4324–17370). From these particles, the particles that had distinct lengths numbered from 419 to 639. The distinct lengths were positively but weakly correlated with the total num-

Table 1
Plugin determined particle size distribution parameters of different ground biomass and rice grain samples from digital images.

Parameter	Pine first thinning	Pine mature stand	Hard wood	Miscanthus	Switchgrass	Elephant grass	Wheat straw	Basmati rice
Total number of particles	7885	4324	15036	4393	10959	17370	4357	741
Image particle area coverage (%)[a]	6.03	7.92	3.88	2.68	2.70	4.36	1.90	15.14
Number particles <9 pixels (%)[b]	70.81	84.41	72.87	76.14	81.04	78.80	68.99	0.00
Number of nonconvex particles (%)	2.18	4.44	2.42	3.00	2.28	2.59	3.51	0.00
Number of distinct particles	538	555	419	462	565	639	444	472
CPU time (ms)	3619	3931	5788	2371	4259	6552	2074	1981
Number of particles analyzed/s	2178	1099	2597	1852	2573	2651	2100	374
D_{95} (mm)	2.441	7.060	1.166	3.306	2.182	2.120	2.815	8.135
D_{90} (mm)	1.554	3.688	0.802	1.502	1.070	1.291	1.899	7.995
D_{84} (mm)	1.060	0.479	0.617	0.800	0.539	0.706	1.238	7.864
D_{75} (mm)	0.587	0.305	0.470	0.429	0.382	0.381	0.691	7.698
D_{60} (mm)	0.323	0.237	0.334	0.293	0.301	0.277	0.340	7.472
D_{50} (mm)	0.262	0.212	0.276	0.253	0.261	0.248	0.266	7.340
D_{30} (mm)	0.200	0.171	0.206	0.201	0.216	0.197	0.209	7.099
D_{25} (mm)	0.185	0.163	0.188	0.187	0.203	0.184	0.194	7.001
D_{16} (mm)	0.161	0.147	0.164	0.163	0.176	0.161	0.167	6.803
D_{10} (mm)	0.146	0.137	0.147	0.147	0.155	0.145	0.149	6.659
D_5 (mm)	0.133	0.128	0.133	0.133	0.137	0.133	0.135	6.418
Uniformity index (%)	8.54	3.48	16.65	8.87	12.83	8.87	7.08	80.28
Size guide number (mm)	26.17	21.21	27.58	25.28	26.09	25.28	26.58	733.96
Size range variation coefficient (%)	171.72	78.32	82.20	125.96	69.54	125.96	201.41	7.22
Relative span	5.38	16.74	2.37	5.36	3.51	5.36	6.58	0.18
Coefficient of uniformity	2.21	1.73	2.27	2.00	1.95	2.00	2.28	1.12
Coefficient of gradation	0.85	0.90	0.87	0.94	1.00	0.94	0.86	1.01
Inclusive graphic skewness	0.79	0.73	0.55	0.77	0.64	0.72	0.82	−0.01
Graphic kurtosis	2.35	19.98	1.50	5.37	4.68	4.14	2.21	1.01

[a] Image particle area coverage (%) = (number of black pixels of particles/total number of pixels of the image) × 100.
[b] Area of nine pixels equals 0.0646 mm^2; and the side of an equivalent square of side 3 pixels equals = 0.2541 mm.

ber of particles (r = 0.41). However, the actual number of distinct particles will decrease with the presence of increased number of similar particles, and vice versa, irrespective of the total number of particles in the sample.

The percentage of nonconvex particles was <4.4% showed the dominant presence of convex particles. The fines dominate among ground biomass particles, as the percentage of finer particles (area <9 pixels) ranged from 69% to 84% (Table 1). Naturally, Basmati rice particles were bigger (0% fines), because the areas of rice studied were in the range from 1014 to 2017 pixels.

The computational speed for the system used (Intel Core2 Duo T5750 @ 2.00 GHz processor; 4.00 GB RAM) was about 374 particles/s for Basmati rice and on average 2150 particles/s for ground biomass. This corresponds to a total computation time for the samples considered of around 6.5 s or less. The computational time increases with increase in the number as well as the projected area of particles.

Ground biomass (non-uniform) and Basmati rice (uniform) particulate material were selected to compare and contrast the samples' determined PSD parameters. For instance, the D_{50} value, quantifying the median length, was greatest for Basmati rice (7.340 mm), and that of ground biomass samples was significantly smaller falling in the narrow range of 0.212–0.276 mm. Similarly, other significant dimension values (D_5 to D_{95}) can be associated with the material studied and compared among others. The various calculated PSD parameters (Table 1) can be interpreted in conjunction with their definitions (Eqs. (1)–(10)). Discussion on some of these parameters was presented later (Section 5.3).

4.4. Mean dimensions of particles

The determined ranges of lengths of particulate biomass were 0.276–0.352 mm for geometric mean (ASABE Standards, S424.2, 2007), 0.280–0.557 mm for graphic mean, and 0.428–1.037 mm for arithmetic average (Table 2). The geometric mean length was smaller than the graphic and the arithmetic mean lengths, while the graphic mean length was in between the other two. The Basmati rice mean lengths were almost constant among the three different means lengths at 7.3 mm, while the width at 1.8 mm.

Obviously, the biomass particles' arithmetic mean width was smaller than their length and it ranged only from 0.157 to 0.248 mm. On average, among the different lengths considered, the length by

Table 2
Range and mean dimensions of samples—all dimensions in mm.

Material	Geometric length[a]	Graphic length[b]	Length[c]			Width[c]		
	$X_{gl} \pm \sigma_{gl}$	$X_g \pm \sigma_{ig}$	Min.	Max.	Mean ± S.D.	Min.	Max.	Mean ± S.D.
Pine first thinning	0.328 ± 2.754	0.494 ± 0.574	0.120	49.050	0.683 ± 1.722	0.083	6.746	0.234 ± 0.336
Pine mature stand	0.276 ± 3.481	0.280 ± 1.133	0.120	23.886	1.037 ± 2.606	0.081	6.635	0.248 ± 0.529
Hard wood	0.289 ± 2.165	0.352 ± 0.270	0.120	19.041	0.428 ± 0.659	0.081	3.505	0.169 ± 0.163
Miscanthus	0.314 ± 2.827	0.405 ± 0.640	0.120	32.199	0.747 ± 1.884	0.083	2.980	0.18 ± 0.209
Switchgrass	0.295 ± 2.312	0.325 ± 0.401	0.120	11.595	0.493 ± 0.808	0.083	2.117	0.157 ± 0.133
Elephant grass	0.314 ± 2.827	0.372 ± 0.437	0.120	32.199	0.747 ± 1.884	0.083	2.980	0.180 ± 0.209
Wheat straw	0.352 ± 2.791	0.557 ± 0.674	0.120	9.750	0.67 ± 0.991	0.081	1.817	0.192 ± 0.186
Basmati rice	7.312 ± 1.076	7.336 ± 0.525	5.286	9.000	7.332 ± 0.525	1.306	2.206	1.758 ± 0.131

[a] Based on ASABE standards S414.1 (2007): X_{gl}, geometric mean length; σ_{gl}, standard deviation of geometric mean length.
[b] Based of Folk and Ward (1957): X_g, graphic mean length; σ_{ig}, inclusive graphic standard deviation of length.
[c] Min., minimum dimension; Max., maximum dimension; S.D., associated standard deviation.

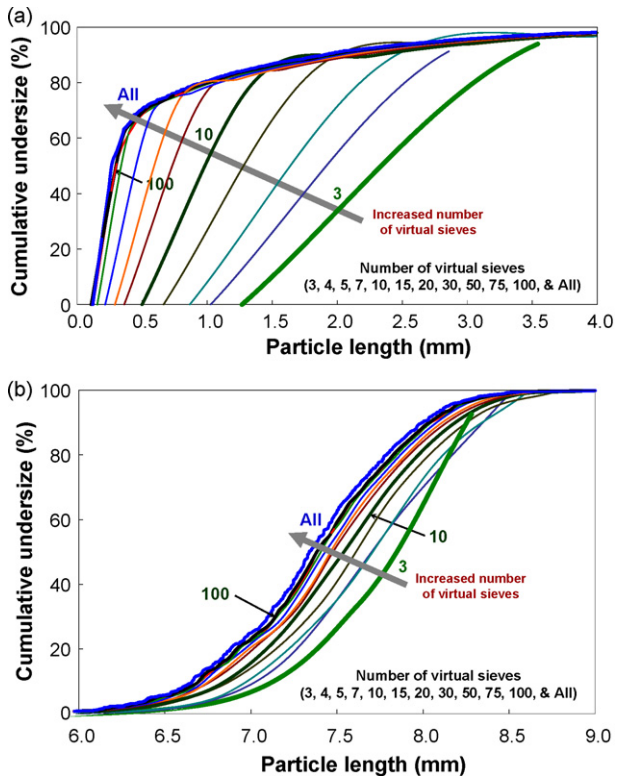

Fig. 8. Cumulative size distribution of typical samples demonstrating the effect of number of equally spaced virtual sieves by simulation in comparison with the all distinct particles of sieveless analysis; (a) wheat straw and (b) Basmati rice.

width ratio of ground biomass was in the range of 1.1–4.2. The length by width ratio of Basmati rice was fairly constant at 4.2.

4.5. Effects of number of sieves by simulation and statistical comparison

Results of simulated cumulative undersize distribution with different number of simulated virtual sieves showed a clear deviation from the sieveless all distinct particles analysis (Fig. 8). The nature of cumulative distribution curves was different for the non-uniform wheat straw ground biomass (Fig. 8a) and uniform Basmati rice particles (Fig. 8b). The separation of curves of number of simulated sieves was greater for ground biomass than that of Basmati rice.

The statistical mean separation analysis revealed that the number of virtual sieves had a significant effect ($P < 0.05$) on most of the PSD parameters of wheat straw particles (Table 3). This can be attributed to the greater variability in the wheat straw particles length. In reference to sieveless analysis, less number of simulated sieves resulted in overestimation of I_u, N_{sg}, X_g, and X_{gl}; and underestimation of S_v, S_l, C_u, C_g, S_{ig}, and K_g. The sieveless analysis coincided with most of the parameters only when the number of sieves equal or greater than 50 sieves. Similar trends (Fig. 8a) and statistical results (Table 3) were also expected with other ground biomass materials characterized by non-uniform particles.

5. Discussion

5.1. Mechanical sieving length-based separation inconsistencies

It can be easily visualized and physically verified that the mechanical sieving produces correct "width-based separation" of the particles. However, the observations and experimental demonstrations (Figs. 3 and 4) emphasize that the length-based separation inconsistency as a definite feature of mechanical sieving. Since mechanical sieving fails in the proper length-based classification of particles, it compromises the accuracy of PSD parameters calculated subsequently.

One way of tackling this inconsistency is to directly measure particle length through computer vision—as followed in this research. When singulated particle arrangements and proper contrast are ensured, then there will not be any length misclassification with the direct measurements through computer vision. The accuracy of measurements can further be improved using increased resolution (DPI) of the image. In addition, the computer vision based application has the advantage of automating the PSD analysis.

5.2. Samples PSD from sieveless analysis

The produced PSD characteristics in such details (Figs. 6 and 7) cannot be achieved by mechanical sieving for want of accuracy in length classification and handling limitation of number of sieves; wherein only a few data points were employed to describe the complete PSD characteristics. However, the computer vision sieveless distinct particle analysis will operate based on the number of distinct particles (≥419; Table 1), which is a variable quantity, unlike a maximum fixed number of sieves (7–10) possible with mechanical sieving.

It should be noted that the PSD curves (Figs. 6 and 7) were based on the number and length of particles, hence will differ from that obtained with mechanical sieving. In general, the PSD curves from mechanical sieving correspond to the mass of material retained on sieves, even though the separation was primarily dimension based. Therefore, in mechanical sieving, the contribution from the finer particles will be subdued as the mass of several finer particles can be equated to a less number of large particles. On the other hand, the sieveless analysis attach equal weight to all particles, irrespective of their size, and therefore the finer particles that are more in number dominate the PSD curve (Fig. 7). It is also possible to construct the mass-based PSD from the sieveless analysis procedure, when relevant volume and density data of the particles are available.

5.3. PSD parameters from sieveless analysis

Allaire and Parent (2003) provided a detailed interpretation of size guide number. The size range variation coefficient can be another useful parameter to readily compare dimension spread, thereby the uniformity of samples. According to size range variation coefficient, Basmati rice (7.22%) has the least dimensional variation while wheat straw (201.41%) had the most (Table 1). For samples with relatively uniform particles such as Basmati rice, the uniformity index and coefficient of uniformity will be closer to 100% and 1.0, respectively, with a relatively smaller spread indicating a narrow length variation. The well distributed non-uniform particles, such as ground biomass, will deviate from the aforementioned values. The developed plugin application can be extended to model PSD and obtain the parameters of common models, such as logarithmic probability, Weibull distribution or Rosin–Rammler, Gates–Gaudin–Schumann, and Gaudin–Meloy (Delagrammatikas and Tsimas, 2004).

Skewness of the distribution is a measure of data asymmetry. A positive inclusive graphic skewness (S_{ig}) represents the presence of increased number of fine particles. According to Folk and Ward (1957) logarithmic original graphical measures classification (Blott and Pye, 2001), the biomass particles ($0.55 \leq S_{ig} \leq 0.82$) can be described as "very finely skewed" as the value ranged between +0.3 to +1.0. While Basmati rice ($S_{ig} = -0.01$) was classified as "symmetrical" since it belonged to the range of +0.1 to −0.1.

Kurtosis is a measure of peadkedness of the distribution. A large value of graphic kurtosis (K_g) indicates the presence of a significant

Table 3
Effect of number of virtual sieves through simulation on the PSD parameters statistically compared with the sieveless all distinct particles analysis.

Material	N	I_u (%)	N_{sg} (mm)	S_v (%)	S_l	C_u	C_g	S_{ig}	K_g	X_g (mm)	X_{gl} (mm)
Wheat straw	3	5.537 a	134.620 a	67.312 c	1.603 d	5.994 b	1.492 a	0.079 j	0.886 f	1.337 a	1.360 a
	4	5.526 a	112.720 g	68.140 c	1.598 d	6.049 b	1.500 a	0.158 e	1.081 c	1.126 g	1.129 g
	5	4.879 b	96.955 b	67.910 c	1.873 h	6.068 b	1.500 a	0.194 i	1.208 g	0.979 b	0.977 b
	7	3.918 c	78.253 c	67.829 c	2.376 i	5.979 b	1.506 a	0.242 h	1.464 e	0.783 c	0.806 c
	10	3.178 d	61.865 d	90.956 e	2.929 g	6.064 b	1.503 a	0.410 g	1.832 d	0.715 d	0.660 d
	15	2.501 e	47.660 e	117.069 f	3.803 f	5.979 b	1.493 a	0.533 f	2.366 b	0.635 e	0.532 e
	20	2.082 f	39.527 f	142.89 d	4.586 e	5.932 b	1.499 a	0.621 d	2.33 b	0.597 ef	0.456 f
	30	1.672 g	31.694 h	183.68 a	5.763 c	6.023 b	1.506 a	0.690 c	2.137 a	0.556 fh	0.385 h
	50	1.332 hi	25.051 ij	233.460 b	7.256 b	6.011 b	1.502 a	0.752 b	2.085 a	0.525 h	0.324 ij
	75	1.290 h	24.316 i	236.026 b	7.538 b	6.905 c	1.323 b	0.768 ab	2.060 a	0.518 h	0.307 i
	100	1.425 i	25.656 ij	224.630 b	7.132 ab	5.671 b	1.569 a	0.756 b	2.090 a	0.528 h	0.309 i
	444[a]	7.169 j	26.640 j	201.716 a	6.601 a	2.289 a	0.857 c	0.822 a	2.202 ab	0.557 fh	0.350 j
Basmati rice	3	78.276 a	741.821 a	8.901 d	0.215 a	1.173 a	1.024 a	1.327 b	0.976 a	7.373 a	7.116 a
	4	77.849 a	723.147 a	8.082 a	0.213 a	1.138 a	1.005 a	0.001 a	–[b]	7.313 a	7.208 a
	5	78.295 a	734.446 a	8.015 ab	0.205 ab	1.139 a	1.013 a	–	1.021 a	7.331 a	7.354 a
	7	78.937 a	732.672 a	7.642 abc	0.194 bc	1.142 a	1.017 a	–	1.039 a	7.401 a	7.276 a
	10	79.254 a	734.302 a	7.46 abc	0.184 c	1.116 a	0.991 a	–	1.041 a	7.266 a	7.256 a
	15	80.979 a	728.776 a	7.373 bc	0.19 bc	1.121 a	1.018 a	–	1.001 a	7.354 a	7.249 a
	20	80.085 a	729.085 a	7.317 c	0.184 c	1.113 a	1.019 a	–	1.011 a	7.312 a	7.396 a
	30	80.680 a	741.887 a	7.311 c	0.185 c	1.135 a	1.006 a	–	0.990 a	7.297 a	7.307 a
	50	80.443 a	727.147 a	7.131 c	0.185 c	1.124 a	1.000 a	–	1.017 a	7.354 a	7.414 a
	75	80.233 a	729.992 a	7.251 c	0.184 c	1.117 a	0.999 a	–	0.999 a	7.393 a	7.241 a
	100	79.559 a	729.375 a	7.319 c	0.184 c	1.112 a	1.024 a	–	1.017 a	7.330 a	7.250 a
	472[a]	80.823 a	726.826 a	7.229 c	0.181 c	1.136 a	1.005 a	–	1.005 a	7.334 a	7.299 a

N, number of virtual sieves; I_u, uniformity index; N_{sg}, size guide number; S_v, sieve range variation coefficient; S_l, relative span; C_u, coefficient of uniformity; C_g, coefficient of gradation; S_{ig}, inclusive graphic skewness; K_g, graphic kurtosis; X_g, graphic mean length; and X_{gl}, geometric mean length. Data represent the back-transformed estimates. Simulated data replications generated based on a random 5.0% variation for mean separation analysis. Dissimilar mean separation group labels (a–j) represent significant difference ($P < 0.05$).

[a] Sieveless analysis based on the total number of distinct particle lengths.

[b] Negative values did not yield mean separation groups.

peak, hence the domination of corresponding size particles. Based on Folk and Ward (1957) classification (Blott and Pye, 2001), pine first thinning, hard wood, and wheat straw ($1.50 \le K_g \le 2.35$) can be classified as "very leptokurtic" having graphic kurtosis in the range of 1.5–3.0; pine mature stand, miscanthus, switchgrass, and elephant grass ($4.14 \le K_g \le 19.985$) as "extremely leptokurtic" having graphic kurtosis >3.0; and Basmati rice ($K_g = 1.01$) as "mesokurtic" since the graphic kurtosis was in the classification range of 0.9–1.11. The positive inclusive graphic skewness and high peaks indicated by the increased graphic kurtosis values were actually due to the presence of increased fine particles.

5.4. Mean dimensions of particles

The geometric mean length was smaller than the arithmetic mean length of the particles (Table 2), because the former gave more weight to dominant finer particles while the latter gave equal weight to all particles. Therefore, geometric mean better represented the particle lengths of samples. The smaller values of geometric mean lengths also explain the associated increased standard deviation when compared to arithmetic mean lengths. The graphic mean also gave more weight to the smaller particles as all the significant dimensions (D_{16}, D_{50}, and D_{84}) of Eq. (7) include the finer particles; hence the resulting lengths were smaller than arithmetic mean lengths. It can also be observed that these three means coincide for uniform particles such as Basmati rice.

The inclusive graphic standard deviations (σ_{ig}) descriptively classify the particulate material based on Folk and Ward (1957) logarithmic original graphical measures classification (Blott and Pye, 2001). The classification obtained from determined values (Table 2) were: hardwood as "very well sorted" ($\sigma_{ig} < 0.35$); switchgrass and elephant grass as "well sorted" ($0.35 \le \sigma_{ig} \le 0.50$); pine first thinning, miscanthus, wheat straw, and Basmati rice as "moderately well sorted" ($0.50 \le \sigma_{ig} \le 0.70$); and pine mature stand as "poorly sorted" ($1.00 \le \sigma_{ig} \le 2.00$). It should be noted these classifications are subjected to change when the same material of the sample were processed under different processing machine settings, such as clearance and product classification screen opening dimensions.

The minimum length and width actually correspond to the dimension of single pixel (a square of 0.0847 mm side), which is the smallest dimension that can be measured with the image resolution used. The maximum length and width along with the minimum dimensions depict the total range of the particles dimensions. Larger values of mean dimensions and smaller values of standard deviation of Basmati rice indicate the particles are larger and more uniform compared to ground biomass.

5.5. Effects of number of sieves by sieving simulation

The sieving simulation that allow selecting virtual sieves offered an insight on PSD, thereby help understanding the effect of number of sieves in sieving procedures. The number "10" in the cumulative undersize characteristics (Fig. 8) indicated the approximate number of sieves that can be handled generally in a single nest of mechanical sieve shakers. Only a close match to the results from sieveless analysis was obtained from sieving results that used more than 50 simulated sieves (75 and 100 sieves).

In addition, it was observed from the sieving simulation that some of the simulated sieves did not retain any material, especially when the number of virtual sieves was large. This happens because some of the particle lengths may not belong to the equally spaced virtual sieve openings assigned. Similar situations may be applicable to mechanical sieving, as the actual PSD may not coincide with the selected sieve openings. On the other hand, the distinct particle sieveless procedure automatically ensures allotment of particles without leaving any gaps. The sieveless all distinct particles analysis was equivalent to an analysis with 444 sieves for wheat straw and 472 sieves for Basmati rice. Clearly, mechanical sieving is physically limited in achieving the correct length-based size distribution.

It is interesting to note with Basmati rice sample that the effect of number of sieves (5% variation replicated data) were not statistically significant ($P < 0.05$), although the analysis produced numerical variation on the PSD parameters. However, simulations with generated data replicated at reduced levels of random variation (3%, 2%, and 1%) showed significant difference ($P < 0.05$) among the number of sieves (data not presented).

These observations lead to the conclusion that mechanical sieving is suitable only when the sample contains uniformly dimensioned particles, and the sieving data had a definite variation ($\geq$5%). This actually represents a very narrow range of particulate material that can be correctly analyzed for PSD by mechanical sieving. The computer vision based sieveless all distinct particles PSD analysis approach can potentially replace the standard mechanical sieving, while providing several advantages, that include accuracy, speed, automated analysis, reproducible results, and low cost. The plugin code can be readily extended to include other PSD parameters and determine parameters of PSD models of particulate material. The plugin can be modified to perform the whole PSD analysis and parameters determination based on width as well with minimal coding effort. We are developing the plugin further to include several possible applications of PSD analysis, and will be uploading the plugin in the ImageJ website after the completion of our planned activities. However, in the meantime, the interested readers can contact the corresponding author by email for the availability of the plugin (some restrictions apply) for academic, scientific, and non-commercial use.

6. Conclusions

This research demonstrated the inconsistencies of length-based separation by mechanical sieving using standard sieves. The passing of particles slightly smaller than twice the opening dimension cannot be avoided irrespective of the wall thickness of the sieve. The maximum deviation observed in particle lengths was in excess of 17 times with respect to opening dimensions of standard sieves. A need for an alternative method for PSD analysis especially for non-uniform particulate materials with a greater particle length:width ratio was established. As demonstrated in this research and previous efforts by Igathinathane et al. (2008a,b, 2009), a computer vision based technique proves to be very capable. The developed user-coded ImageJ plugin, based on all particles of distinct lengths of the sample, successfully determined PSD parameters of ground biomass particles and Basmati rice without the need for sieving. Image-based sieve simulation indicated significant effect ($P < 0.05$) on number of sieves used in PSD analysis, especially for non-uniform material such as ground biomass. More than 50 equally spaced sieves were required for non-uniform particles to match the results of sieveless all distinct particles approach; which was not practical with mechanical sieving due to handling limitations. Particulate material PSD and the various derived parameters associated with the distribution and the models based on a limited manageable number of sieves (e.g. less than 10 sieves) in a common mechanical sieve shaker, which already shown to be not accurate with length classification, may constitute a major drawback of the standard mechanical sieving method. The developed computer vision plugin determined several useful dimensions and parameters representative of material PSD and provided rapid analysis with a processing rate greater than or equal to 1099 ground biomass or and 374 Basmati rice particles per second. This computer vision PSD approach is a superior means to perform PSD analysis and can potentially replace mechanical sieving. Mass-based PSD utilizing particle density and volume data as well as width-based PSD analyses can be easily incorporated into the plugin. Moreover, the computer vision plugin provides several advantages over mechanical sieving, such as accuracy, speed, low cost, automated analysis, reproducible results, and can be readily extended to model (e.g., Rosin–Rammler) the PSD of materials.

Acknowledgements

This research was supported by the Sustainable Energy Research Center and the Mississippi Agricultural and Forestry Experiment Station at Mississippi State University with funds provided by the U.S. Department of Energy under Award No. DE-FG3606GO86025. This support is gratefully appreciated. Thanks are also due to William Massey and Kyle Thomas for undertaking the grinding of the bulk biomass materials from which the test samples were obtained.

References

Allaire, S.E., Parent, L.E., 2003. Size guide and Rosin–Rammler approaches to describe particle size distribution of granular organic-based fertilisers. Biosyst. Eng. 86, 503–509.

Allais, I., Edoura-Gaena, R.B., Gros, J.B., Trystram, G., 2006. Influence of egg type, pressure and mode of incorporation on density and bubble distribution of a lady finger batter. J. Food Eng. 74, 198–210.

ASABE Standards, 2007. Method of Determining and Expressing Particle Size of Chopped Forage Materials by Screening—ANSI/ASAE S424.1 MAR1992 (R2007). ASABE Standards 2008. ASABE, St. Joseph, MI.

Bailer, W., 2006. Writing ImageJ Plugins—A Tutorial. Version 1.71. http://rsb.info.nih.gov/ij/download/docs/tutorial171.pdf (Accessed February, 2009).

Blott, S.J., Pye, K., 2001. GRADISTAT: A grain size distribution and statistics package for the analysis of unconsolidated sediments. Earth Surf. Process. Landforms 26, 1237–1248.

Brosnan, T., Sun, D.W., 2002. Inspection and grading of agricultural and food products by computer vision systems—a review. Comput. Electron. Agric. 36, 193–213.

Burger, W., Burge, M.J., 2008. Digital Image Processing—An Algorithmic Introduction using Java. Springer, New York, N.Y.

CFI, 2001. Bulk Blend. Quality Control Manual. Canadian Fertilizer Institute, Ontario, Canada.

Craig, R.F., 2004. Craig's Soil Mechanics. Spon Press, London.

Cruvinel, P.E., Vieira, S.R., Crestana, S., Minatel, E.R., Mucheroni, M.L., Neto, A.T., 1999. Image processing in automated measurements of raindrop size and distribution. Comput. Electron. Agric. 23, 205–217.

Delagrammatikas, G., Tsimas, S., 2004. Grinding process simulation based on Rosin–Rammler equation. Chem. Eng. Commun. 191, 1362–1378.

EBA, 1997. Handbook of Solid Fertilizer Blending. Code of Good Practices for Quality. European Blenders Association Le Pontoury, Montviron, France.

Folk, R.L., Ward, W.C., 1957. Brazos River bar: a study in the significance of grain size parameters. J. Sediment. Petrol. 27, 3–26.

Igathinathane, C., Pordesimo, L.O., Batchelor, W.D., 2008a. Ground Biomass Sieve Analysis Simulation by Image Processing and Experimental Verification of Particle Size Distribution. ASABE Paper No. 084126. ASABE, St. Joseph, MI.

Igathinathane, C., Pordesimo, L.O., Columbus, E.P., Batchelor, W.D., Methuku, S.R., 2008b. Shape identification and particles size distribution from basic shape parameters using ImageJ. Comput. Electron. Agric. 63, 168–182.

Igathinathane, C., Pordesimo, L.O., Batchelor, W.D., 2009. Major orthogonal dimensions measurement of food grains by machine vision using ImageJ. Food Res. Int. 42, 76–84.

Maerz, N.H., 1998. Aggregate sizing and shape determination using digital image processing. In: Center for Aggregates Research (ICAR) Sixth Annual Symposium Proceedings, St. Louis, Missouri, April 19–20, pp. 195–203.

Momota, M., Miike, H., Hashimoto, H., 1994. Measuring particle size distribution by digital image processing with inverse Fourier–Bessel transformation. Jpn. J. Appl. Phys. 33, 1189–1194.

Mora, C.F., Kwan, A.K.H., Chan, H.C., 1998. Particle size distribution analysis of coarse aggregate using digital image processing. Cem. Concr. Res. 28, 921–932.

Rasband, W.S., 2007. ImageJ. U.S. National Institutes of Health, Bethesda, MD, USA, http://rsb.info.nih.gov/ij/index.html (Accessed February, 2009).

Rodieck, B., 2008. EllipseFitter Class of ImageJ, Available at: http://rsb.info.nih.gov/ij/developer/source/ij/process/EllipseFitter.java.html (Accessed February, 2009).

Saxton, A.M., 2003. Mixed Model ANOVA Analysis Macro. University of Tennessee, Knoxville, TN 37996-4574.

Shahin, M.A., Symons, S.J., 2005. Seed sizing from images of non-singulated grain samples. Can. Biosyst. Eng. 47, 49–54.

Shahin, M., Symons, S.J.S., Poysa, V., 2006. Determining soya bean seed size uniformity with image analysis. Biosyst. Eng. 94, 191–198.

Visen, N.S., Paliwal, J., Jayas, D.S., White, N.D.G., 2004. Image analysis of bulk grain samples using neural networks. Can. Agric. Eng. 46, 11–15.

Womac, A.R., Igathinathane, C., Bitra, P., Miu, P., Yang, T., Sokhansanj, S., Narayan, S., 2007. Biomass Pre-processing Size Reduction with Instrumented Mills. ASABE Paper No. 076046. ASABE, St. Joseph, MI.